A cytoskeletal network maintains filament shape in the multicellular cyanobacterium *Anabaena sp.* PCC 7120

Benjamin L. Springstein[1*], Dennis J. Nürnberg[2,†], Ann-Katrin Kieninger[3], Christian Woehle[1], Julia Weissenbach[1,‡], Marius Theune[1], Andreas O. Helbig[4], Andreas Tholey[4], Iris Maldener[3], Tal Dagan[1], Karina Stucken[5*+]

[1] Institute of General Microbiology, Christian-Albrechts-Universität zu Kiel, Kiel, Germany

[2] Department of Life Sciences, Imperial College, London SW7 2AZ, United Kingdom

[3] Department of Microbiology/Organismic Interactions, University of Tübingen, Tübingen, Germany

[4] AG Proteomics & Bioanalytics, Institute for Experimental Medicine, Christian-Albrechts-Universität zu Kiel, Kiel, Germany

[5] Department of Food Engineering, University of La Serena, La Serena, Chile.

[†] Present address: Institute of Experimental Physics, Free University of Berlin, Berlin, Germany

[‡] Present address: Faculty of Biology, Technion-Israel Institute of Technology, Haifa, 32000, Israel

* Corresponding authors: KS kstucken@userena.cl; BLS bspringstein@ifam.uni-kiel.de

[+] lead author: Karina Stucken

Bacterial cell shape is an important determinant of the organism physiology, its interaction with the environment and the coordination of myriad intracellular processes[1]. The cell shape is determined by peptidoglycan (PG) biogenesis and its spatial distribution, which is coordinated by components of the bacterial cytoskeleton[2]. Those proteins typically self-associate into polymers and interlink into higher-order structures in the cell[2]. Two of the major determinants of bacterial cell shape are extensively studied in unicellular forms; examples are MreB that functions in cell wall synthesis[3] and FtsZ, which mediates cell division[4]. Nonetheless, the mechanisms that shape bacterial multicellular forms remain understudied. Here we report a novel cytoskeletal network that determines filament shape and viability in the multicellular cyanobacterium *Anabaena sp.* PCC 7120 (hereafter *Anabaena)*. Studying coiled-coil rich proteins (CCRPs) in *Anabaena*, we identified two proteins – Alr4504 and Alr4505 (named LfiA and LfiB for linear filament) – that assemble into a heteropolymer traversing the longitudinal cell axis. Two additional CCRPs, Alr0931 (named CypS for cyanobacterial polar scaffold) and All2460 (named CeaR for cyanobacterial elongasome activity regulator), are localized at the cell poles and cell wall, respectively. Deletion mutants show impaired filament and cell shapes and a decreased filament viability. The four proteins interact with each other, with SepJ[5] and MreB; thus they form a proteinaceous network that stabilizes the *Anabaena* multicellular filament through direct interactions with the septal junctions and the cell wall. We propose that this cytoskeletal network is essential for the manifestation of a multicellular phenotype in *Anabaena*. Our study reveals a function of the bacterial cytoskeleton in the maintenance of multicellular forms in prokaryotes.

Bacterial multicellularity ranges from transient associations, such as colonies and biofilms to permanent multicellular forms[6]. A key hallmark of permanent bacterial multicellularity is a well-defined and reproducible shape, termed patterned multicellularity[7]. Patterned multicellular structures are the result of either coordinated behavior as in myxobacteria[8], or cell division, proliferation and cell differentiation as in sporulating actinomycetes[9] and cyanobacterial

filaments[10,11]. Filamentous cyanobacteria that differentiate multiple cell types are considered the peak of prokaryotic complexity and their cell biology has been studied in the context of cytoplasmic continuity, intercellular communication, and cell differentiation[12]. Species of the Nostocaceae are characterized by a formation of linear filaments, where equally interspaced heterocysts are differentiated upon nitrogen starvation[12]. Studies of multicellular growth in the model multicellular cyanobacterium *Anabaena* showed that FtsZ is an essential protein and localizes to future septum sites in a typical Z-ring structure, while MreB determines the cell shape of a single cell within an *Anabaena* filament but is dispensable for filament viability[13,14]. Intercellular communication in *Anabaena*[15] is facilitated by direct cell connections, the septal junctions, involving septum localized proteins SepJ, FraC and FraD[5,16] and a nanopore array in the septal peptidoglycan[17].

To study the role of cytoskeletal proteins in *Anabaena* patterned multicellularity, we performed a computational prediction of filament-forming proteins by surveying CCRPs, putative IF-like proteins[18], encoded in the *Anabaena* genome. This resulted in 186 CCRPs (Supplementary File 1) that were further filtered to include only hypothetical proteins of unknown function, yielding a set of 13 candidates for further research (Supplementary Fig. 1 and Supplementary Table 1). The domain structure of the 13 candidates showed the canonical unstructured head and tail domains characteristic to eukaryotic proteins forming intermediate filaments (IFs)[18] and prokaryotic IF-like proteins[19]. The distribution of homologs to these candidates in cyanobacteria showed that eight CCRPs are distributed in unicellular and non-heterocystous cyanobacteria while four CCRPs are present only in multicellular cyanobacteria (Fig. 1a; Supplementary Table 1).

To evaluate the ability of candidate CCRPs to self-associate, an essential property of cytoskeletal proteins, we ectopically expressed C and N-terminally tagged (His6, eCFP or GFP) recombinant proteins and investigated *in vitro* polymerization properties and *in vivo* localization pattern. For the *in vitro* polymerization assay, we purified His-tagged proteins by Ni-NTA affinity chromatography under denaturing conditions and renatured them by dialysis

followed by NHS-fluorescein staining. Four out of thirteen proteins showed self-association characteristics, including LfiA, LfiB, CypS and All4981 (that will be investigated in a separate report). Accordingly, those proteins were classified as filament-forming. Candidates that failed to form filamentous structures *in vivo* and *in vitro* were excluded from further analysis, except for CeaR whose structural prediction, reminiscent of the well-characterized prokaryotic IF-like protein crescentin[19], showed significant similarity to EzrA[20] (Supplementary Table 1). The four studied proteins were expressed under standard growth conditions (Supplementary Fig. 2a).

An inspection of the genomic loci suggested that *lfiA* and *lfiB* are encoded in an operon structure, although RT-PCR data suggests that they are not co-transcribed (Supplementary Fig. 2b). LfiA and LfiB alone failed to polymerize *in vitro* (Fig. 1b), while both proteins are able to heteropolymerize, forming a circular meshwork of filaments (Fig. 1c). To examine their *in vivo* localization pattern, we expressed translational GFP fusions of both proteins in *Anabaena* wildtype (WT). The expression of LfiA-GFP and LfiB-GFP from the native promoter revealed no discernible expression of LfiB-GFP (Supplementary Fig. 3a). Consequently, we investigated the *in vivo* localization of both proteins from the copper-inducible *petE* promoter. This showed that both proteins do not form filamentous structures when expressed independently (Fig. 1d), however, co-expression of LfiA-eCFP and LfiB-GFP resulted in a distinct polymer along the longitudinal cell axis (Fig. 1e). The intracellular localization of LfiA/LfiB filaments suggests that the proteins are anchored at the cell poles and do not cross cell-cell borders (Figs. 1e inlay and 1f). These results demonstrate that LfiA and LfiB are interdependent for polymerization and form a heteropolymer *in vivo* and *in vitro*. The co-polymerization of LfiA and LfiB was also verified by heterologous expression in an Δ*lfiA*Δ*lfiB* double mutant background and in *E. coli* (Supplementary Fig. 3b,c and 5).

In vitro polymerization of CypS revealed short filamentous strings (Fig. 1b). Notably, no expression of CypS-GFP from P_{cypS} was detected in the WT (Supplementary Fig. 4a). However, when expressed from P_{cypS} in the *ΔcypS* mutant strain or from P_{petE} in the WT strain, CypS-GFP was localized to the cell periphery and the cytosol (Supplementary Fig. 4a). In

contrast, expression of CypS-GFP in *E. coli* and immunolocalization of CypS-His in *Anabaena* revealed the protein to form large plugs at the cell poles (Fig. 1g, Supplementary Fig. 4b) that appear to displace the thylakoid membranes (Supplementary Fig. 4c). Furthermore, overexpression of CypS-His induced cell swelling (Supplementary Fig. 4c), indicating that CypS has morphogenic properties and possibly functions as a scaffold protein for the anchorage of other proteinaceous structures, including the LfiA-eCFP/LfiB-GFP heteropolymer (Supplementary Fig. 5).

For the examination of CeaR polymerization we used the same approach as for the proteins described above, however, no filamentous *in vitro* structures were observed. Notably, recombinant expression of CeaR-GFP in *Synechocystis* was unsuccessful. This, together with the absence of homologs to CeaR in unicellular cyanobacteria (Fig. 1a) suggested that CeaR function is related to the multicellular cyanobacterial phenotype. Expression of CeaR-GFP from P_{ceaR} and P_{petE} in *Anabaena* showed that the protein localizes primarily to the cell periphery in a patchy pattern (Fig. 1h, Supplementary Fig. 6a). However, CeaR-GFP also accumulated near the septa or associated with the Z-ring, leading to a swollen cell phenotype of a proportion of cells within the filament (Fig. 1h, Supplementary Fig. 6a). The localization pattern suggests that CeaR might be associated with the FtsZ-driven divisome. Z-ring localization was lost upon removal of the N-terminal transmembrane domains, indicating that membrane anchorage is key for proper CeaR function (Supplementary Fig. 6a). Enlarged cells in an *Anabaena* filament have previously been observed in the context of an overexpressed *mreBCD* operon[14], hinting for a similar function in longitudinal PG synthesis.

To further study the function of the four CCRPs, we generated Δ*cypS,* Δ*ceaR* and a double Δ*lfiA*Δ*lfiB* mutant strain and examined their phenotype. Notably, single Δ*lfiA* or Δ*lfiB* mutant strains could not be generated. Our results show that all deletion strains were characterized by altered filament or cell shape phenotypes and viability (Fig 2a,b, Supplementary Fig. 7a,b). The Δ*cypS* and Δ*lfiA*Δ*lfiB* mutants showed filaments that displayed a zigzagged instead of a linear growth pattern (Fig. 2a). Additionally, Δ*cypS* and Δ*lfiA*Δ*lfiB* cells

were significantly larger in comparison to the WT, while Δ*ceaR* cells were significantly smaller than the WT (Fig. 2c). The decreased cell volume in the Δ*ceaR* strain is in accordance with our observation of cell volume increase when overexpressing CeaR in the WT (Figs. 1h, Supplementary Fig. 6a). The effect of CeaR level on cell shape reinforces a role of CeaR in PG biogenesis and cell-shape determination. Furthermore, cells in both Δ*cypS* and Δ*lfiA*Δ*lfiB* mutants exhibited a significantly more rounded cell phenotype (Fig. 2c), reminiscent of the Δ*mreB* mutant[14].

Round and swollen cell phenotypes are indicative of an impairment in cell wall integrity and defects in PG biogenesis as well as an elevated sensitivity to turgor pressure[21–24]. This raised the hypothesis that the four investigated CCRPs could be involved in cell wall integrity. Consequently, we tested the sensitivity of the deletion strains to cell wall degrading enzymes and osmotic stressors. The Δ*cypS* mutant had elevated sensitivity to lysozyme, and both Δ*cypS* and Δ*lfiA*Δ*lfiB* mutants were more sensitive to Proteinase K compared to the WT and the Δ*ceaR* mutant (Fig. 2d). This observation suggests a defect in cell wall integrity for both strains. Increased sensitivity to lysozyme has also previously been associated with a defect in elongasome function[14], suggesting that CypS could be associated with the *Anabaena* elongasome. Furthermore, Δ*cypS* and Δ*lfiA*Δ*lfiB* mutants were unable to grow in liquid culture with Δ*cypS* mutant cells rapidly bursting upon transfer to liquid culture, hinting for an elevated sensitivity to fluid shear stress or turgor pressure (Supplementary Fig. 8a,b). In addition to the decreased cell volume, we also observed a similar, albeit mitigated reduction of filament viability for the Δ*ceaR* mutant strain (Fig. 2b, Supplementary Figs. 8a and 9). Upon nitrogen stepdown, the Δ*ceaR* mutant fragmented into shorter filaments that aggregated into large-scale cell clumps (Fig. 2b). Additionally, the observed loss of chlorophyll signal showed that these filaments lost viability and died within a few days (Supplementary Fig. 9). Mutants of genes involved in intercellular communication in *Anabaena* show a similar phenotype when grown without nitrogen due to the loss of diazotrophy[5,25]. Proper nutrient exchange through septal junctions is essential for *Anabaena* viability, especially under diazotrophic growth[12]. Consequently, we investigated the level of intercellular communication using FRAP

experiments of all mutant strains. Our results show that the Δ*lfiA*Δ*lfiB* mutant is not impaired in intercellular solute diffusion while diffusion is reduced in the Δ*cypS* mutant and virtually absent in the Δ*ceaR* mutant grown in liquid medium (Fig. 2e, Supplementary Figs. 10 and 11). Notably, solute diffusion was unaltered in young Δ*ceaR* mutant cells grown on BG11 plates, indicating a culture-age dependent effect (Fig. 2e). To further investigate the underlying cause for the impaired cell-cell communication, we isolated sacculi and observed that the Δ*ceaR* and the Δ*cypS* mutant partially contain significantly larger septa with decreased nanopore counts compared to the WT, suggesting that those septa could be responsible for the decrease in solute diffusion (Supplementary Fig. 12).

Except for Δ*ceaR* cells that contain a red fluorescent filament (Supplementary Fig. 7d), ultrastructures of the mutant strains were largely unaffected regardless of their impact on filament viability (Supplementary Fig. 13). However, the observed cell wall defects and altered cell shape phenotypes indicates that CypS, LfiA/B and CeaR function is involved in PG biogenesis and suggests a connection to the FtsZ-driven divisome or MreB-driven elongasome[2]. To test for a link with the divisome, we visualized Z-ring placement in the WT and each of the mutant strains by immunofluorescence. No alterations in Z-ring placement nor DNA localization were observed, indicating that Z-ring formation and nucleoid structure are unaffected (Supplementary Figs. 14 and 15). To test for a link with the elongasome, we compared the MreB localization in cells ectopically expressing GFP-MreB from P_{petE} or the native MreB promoter (we note that GFP-MreB expression from the native promoter had a strong negative effect on *Anabaena* viability; Supplementary Fig. 16). The P_{mreB}-driven expression of GFP-MreB revealed the formation of GFP-MreB aggregates (Supplementary Fig. 16b), in a pattern that differs considerably from previous observations on the MreB localization using P_{petE}::*gfp-mreBCD*[14]. Expression of GFP-MreB in the mutants revealed considerable alterations of MreB localization compared to the single filaments observed in the WT (Fig 3a, Supplementary Fig. 16b). In the Δ*ceaR* mutant, GFP-MreB mainly localized as spot-like structures and only rarely formed bundles as observed in the WT (Fig. 3d), showing that MreB polymerization is diminished in the Δ*ceaR* mutant. The inhibitory effect on MreB

polymerization became even more evident during growth in liquid culture where GFP-MreB filaments were never observed and Δ*ceaR* mutant cells showed a defect in cell and filament shape with a prominent zigzagged filament growth (Fig. 3d). Despite being expressed from P_{petE}, GFP-MreB signal intensity was strongly elevated in these cells, which suggests a role of CeaR in MreB turnover. Further indication for an involvement of CeaR in MreB function is provided by the ectopic localization of CeaR-GFP in *E. coli*, which showed a banded and helical pattern (Supplementary Fig. 6b) resembling that of YFP-MreB[26]. In the Δ*cypS* mutant, GFP-MreB localization resembled the WT localization (Fig. 3c). GFP-MreB filaments were also present in the Δ*lfiA*Δ*lfiB* mutant, being primarily detected in non-rounded cells having a WT-like phenotype (Fig 3b inlay) whereas in rounded cells of zigzagged filaments, the GFP-MreB signals were restricted to the cell poles (Fig. 3b). These observations suggest that LfiA and LfiB are important for the function and localization of MreB.

To further assess the function of *Anabaena* CCRPs in PG turnover, we stained active PG synthesis by fluorescently-labeled vancomycin (Van-FL). This revealed alterations in the PG remodeling between WT and CCRP mutant strains (Fig. 3e,f). The Δ*ceaR* mutant is characterized by an increased mean intensity of Van-FL staining that is observed not only in the septal wall as in the WT but also in the lateral cell wall (Fig. 3e). Consequently,we suggest that CeaR acts as a regulator PG biogenesis and/or localization of the PG biogenesis machinery. This is in agreement with the altered expression and localization pattern of GFP-MreB in the Δ*ceaR* mutant (Fig. 3d). Nonetheless, Δ*lfiA*Δ*lfiB* and Δ*cypS* mutants showed a similar Van-FL staining pattern to the WT albeit with reduced staining intensity (Fig 3e,f), hence it is likely that also CypS, LfiA and LfiB are linked to PG biogenesis. The suggested role of the four CCRPs in PG turnover is furthermore in agreement with the observed swollen cell phenotype in the Δ*cypS* and Δ*lfiA*Δ*lfiB* mutant and with the altered MreB localization in the mutant strains. As we saw that CCRP mutants affect cell wall integrity, we tested if the formation of the heterocyst polysaccharide layer is impaired in the mutants. However, staining with alcian blue, which specifically binds to heterocyst polysaccharides, showed that all mutants developed mature heterocysts (Supplementary Fig. 17).

As *Anabaena* CCRP mutant strains displayed similar phenotypes and the four *Anabaena* CCRPs were all linked to MreB function and PG turnover, we investigated whether those proteins interact with each other and with other known morphological determinants in *Anabaena*. Bacterial two hybrid assays revealed that all four CCRPs are able to self-interact (Fig 4a), thus confirming the *in vitro* polymerization assays (Fig. 1b,c). Additionally, all four CCRPs were able to cross-interact with each other (Fig. 4a). We found that LfiA, LfiB and CeaR but not CypS, interact with MreB. Additionally, CeaR weakly interacts with FtsZ (Fig. 4a, Supplementary Fig. 19), which is in agreement with the Z-ring-like *in vivo* localization of CeaR-GFP (Fig. 1i, Supplementary Fig. 6a). Furthermore, all proteins were identified as interaction partners of the septal protein SepJ, but not with FraC and FraD (Fig. 4a). Our results were verified by co-immunoprecipitation assays followed by LC-MS/MS analytics. This revealed further interactions of CeaR with MinD and ParA (two known cytoskeletal proteins[27]) and three penicillin binding proteins (regulators of PG synthesis[28]), corroborating a role of CeaR in PG biogenesis (Supplementary Fig. 18 and Supplementary File 3).

Our results demonstrate the capacity of the four CCRPs to form an interconnected cytoskeletal network in *Anabaena*. The network is anchored to the cell poles and likely relays stabilizing properties to neighbouring cells, thus maintaining the linear filament phenotype. (Fig. 4b). The conserved combination of all four CCRPs in heterocystous cyanobacteria that form linear (or false branching; Fig. 1a) filaments suggests that the linear filament formation has a selective advantage. While the selective advantage of cell shape is considered to be mostly a manifestation of biotic and abiotic selective factors in the cell environment[1], the selective advantage of multicellular shapes is likely related to the efficiency of intercellular communication and transport[29]. Indeed, the results of our FRAP experiments show that the efficiency of flow in the zigzagged filament is reduced. The evolution of patterned multicellularity is considered an important step towards a sustainable division of labor and the development of cell differentiation[7]. Our study reveals the role of cytoskeletal proteins in the evolution and maintenance of bacterial multicellular form.

Acknowledgments

We thank Katrin Schumann, Myriam Barz, Lisa Stuckenschneider, Lisa-Marie Philipp and Claudia Menzel for their assistance in the experimental work. We thank Tanita Wein for critical comments on the manuscript. FRAP experiments were done at the Facility for Imaging by Light Microscopy (FILM) at Imperial College London. We thank Tine Pape for assistance with graphic illustrations (funded by the cluster of excellence ‘‘The Future Ocean’’ at Kiel University). The study was supported by the German science foundation (DFG) (Grant No. STU513/2-1 awarded to KS). DJN was supported by the BBSRC as part of the joint NSF Ideas Lab grant on ‘Nitrogen: improving on nature’ (grant BB/L011506/1). IM and AK were supported by German science foundation (DFG) (Grant SFB766).

Author contribution

BLS and KS designed the study. BLS established and performed the experimental work with contributions from MT and JW. CW and TD performed comparative genomics analysis. DJN and AKK performed FRAP assays and AKK and IM carried out ultrathin structures and nanopore analyses. AOH and AT analyzed protein samples by mass spectrometry. BLS, TD and KS drafted the manuscript with contributions from all coauthors.

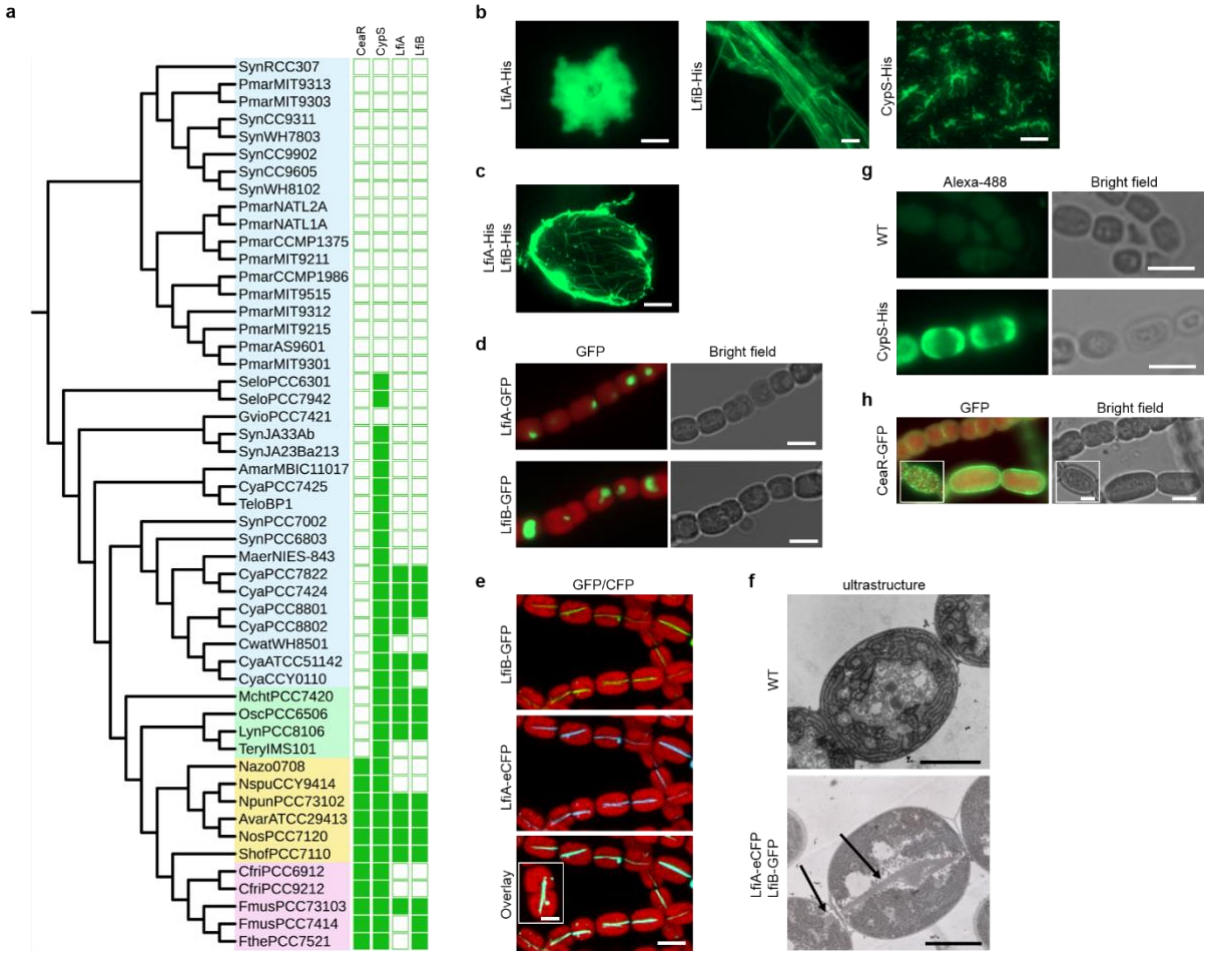

Fig. 1: Cyanobacterial CCRPs polymerize *in vitro* and *in vivo*

(**a**) Distribution of protein candidate homologs in cyanobacteria. Organism names include the genus first letter and species first three letters. The presence of homologous genes is marked by a green rectangle. Organism names are shaded according to cell or colony morphology; blue: unicellular, green: filamentous, yellow: filamentous and heterocyst forming, pink: heterocyst forming and true branching or multiseriate filaments. Homologs accession numbers are supplied in Supplementary File 2. (**b**-**c**) Epifluorescence micrographs of NHS-Fluorescein-stained *in vitro* filaments formed by purified and renatured (**b**) LfiA-His (1 mg ml^{-1}), LfiB-His (0.5 mg ml^{-1}) and CypS-His (0.5 mg ml^{-1}) or (**c**) co-renatured LfiA-His and LfiB-His (0.25 mg ml^{-1} each) in 25 mM HEPES, pH 7.4 (LfiB), HLB (LfiA and co-renatured LfiA/B) or PLB (CypS) renaturation buffer. (**d**) Merged GFP-fluorescence and chlorophyll autofluorescence (red) and bright field micrographs of *Anabaena* WT cells expressing LfiA-GFP or LfiB-GFP from P_{petE}. LfiA-GFP-expressing cells were grown in BG11 without copper and induced for 2 d with 1 µM $CuSO_4$. FisB-GFP-expressing cells were grown in BG11-0. (**e**) Merged GFP and/or eCFP fluorescence and chlorophyll autofluorescence (red) micrographs of *Anabaena* WT cells co-expressing LfiA-eCFP and LfiB-GFP from P_{petE} and grown in BG11-0. (**f**) Electron micrographs of ultrathin sections of *Anabaena* WT and *Anabaena* cells co-expressing LfiA-eCFP and LfiB-GFP grown in BG11. Black arrows indicate electron-dense structures coinciding with the LfiA/B heteropolymer observed in Fig. 1e. Filaments appear to anchor to the cell poles. (**g**) Alexa Fluor 488 and bright field micrographs of anti-His immunofluorescence staining of *Anabaena* WT and *Anabaena* cells expressing CypS-His from P_{petE} grown in liquid BG11-0 supplemented with 0.25 µM $CuSO_4$ for 2 d. Polar sites loaded with CypS-His plugs coincide with sites of retracted chlorophyll autofluorescence observed prior to immunofluorescence (Supplementary Fig. 4c). (**h**) Merged GFP fluorescence and chlorophyll autofluorescence and bright field micrographs of *Anabaena* WT cells expressing CeaR-GFP from P_{petE} grown on BG11. Notably, no enlarged cells were identified in the Δ*ceaR* mutant strain expressing CeaR-GFP from P_{ceaR} (Supplementary Fig. 6a), indicating that CeaR level in WT cells is tightly regulated. Inlay shows patchy and cell periphery-localized CeaR-GFP. N-terminal YFP translational fusion of CCRPs did not reveal coherent structures, suggesting that the N-terminus is essential for protein localization. Scale bars: 5 µm, (e) 1.25 µm, (f) 1.6 µm or (h inlay) 2.5 µm.

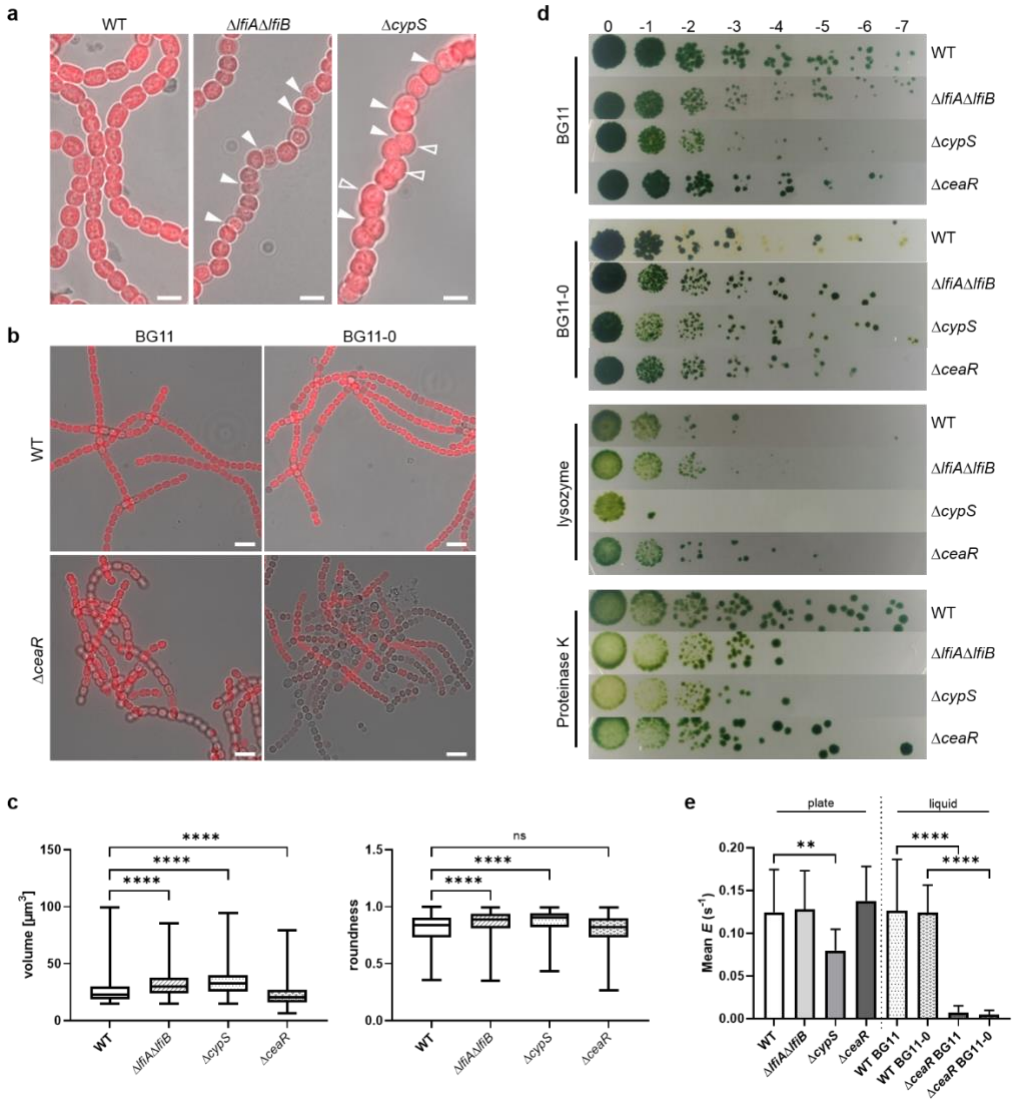

Fig. 2: *Anabaena* CCRP mutant strains reveal altered filament and cell shape phenotypes

(**a**-**b**) Merged chlorophyll autofluorescence and bright field micrographs of (**a**) *Anabaena* WT, Δ*lfiA*Δ*lfiB* and Δ*cypS* mutant strains grown on BG11 plates and (**b**) *Anabaena* WT and Δ*ceaR* mutant strain grown in BG11 and 5 days after transfer into BG11-0. Reduced Δ*ceaR* filament viability was also observed during prolonged cultivation on BG11 plates (Supplementary Fig. 7c). Unlike in the WT, we commonly observed bright red fluorescent filaments in the Δ*ceaR* mutant (Fig. 3d, Supplementary Fig. 7d). Notably, ultrastructures revealed that those structures do not consist of thylakoid membranes (Supplementary Fig. 13), leaving the nature of those filaments unknown. White triangles indicate zigzagged growth and translucent triangles show swollen cells. Scale bars: (a) 5 µm and (b) 10 µm. (**c**) Cell roundness and volume of *Anabaena* WT, Δ*lfiA*Δ*lfiB*, Δ*cypS* and Δ*ceaR* mutant strains grown on BG11 plates measured with Fiji imaging software. *Anabaena* WT: n = 537; Δ*ceaR*: n = 796; Δ*lfiA*Δ*lfiB*: n = 404; Δ*ceaR*: n = 369. (**d**) *Anabaena* WT, Δ*lfiA*Δ*lfiB*, Δ*cypS* and Δ*ceaR* mutant strains were were spotted onto BG11 and BG11-0 plates or BG11 plates supplemented with lysozyme or Proteinase K in triplicates of serial dilutions of factor 10 and grown until no further colonies arose in the highest dilution (n = 2). (**e**) Mean exchange coefficients (*E*) of fluorescence recovery after photobleaching (FRAP) experiments from calcein-labelled *Anabaena* WT and *Anabaena* mutant strains. Liquid *Anabaena* WT and Δ*ceaR* cultures were grown in BG11 and partially transferred to BG11-0 1 d prior labelling. Plate grown *Anabaena* WT, Δ*lfiA*Δ*lfiB* and Δ*cypS* mutant strains were grown on BG11 plates. *Anabaena* WT BG11 plate: n = 21; *Anabaena* WT liquid BG11: n = 10; *Anabaena* WT liquid BG11-0: n = 11; Δ*cypS*: n= 23; Δ*lfiA*Δ*lfiB*: n = 17; Δ*ceaR* liquid BG11: n = 16; Δ*ceaR* liquid BG11-0: n = 6. Representative FRAP micrographs are shown in Supplementary Fig. 10. Representative fluorescence recovery curves are shown in Supplementary Fig. 11. Values indicated with * are significantly different from the WT. *: $P < 0.05$, **: $P < 0.01$, ***: $P < 0.001$, ****: $P < 0.0001$. ns indicates no significant different to the WT (using one-way ANOVA with Dunnett's multiple comparison test).

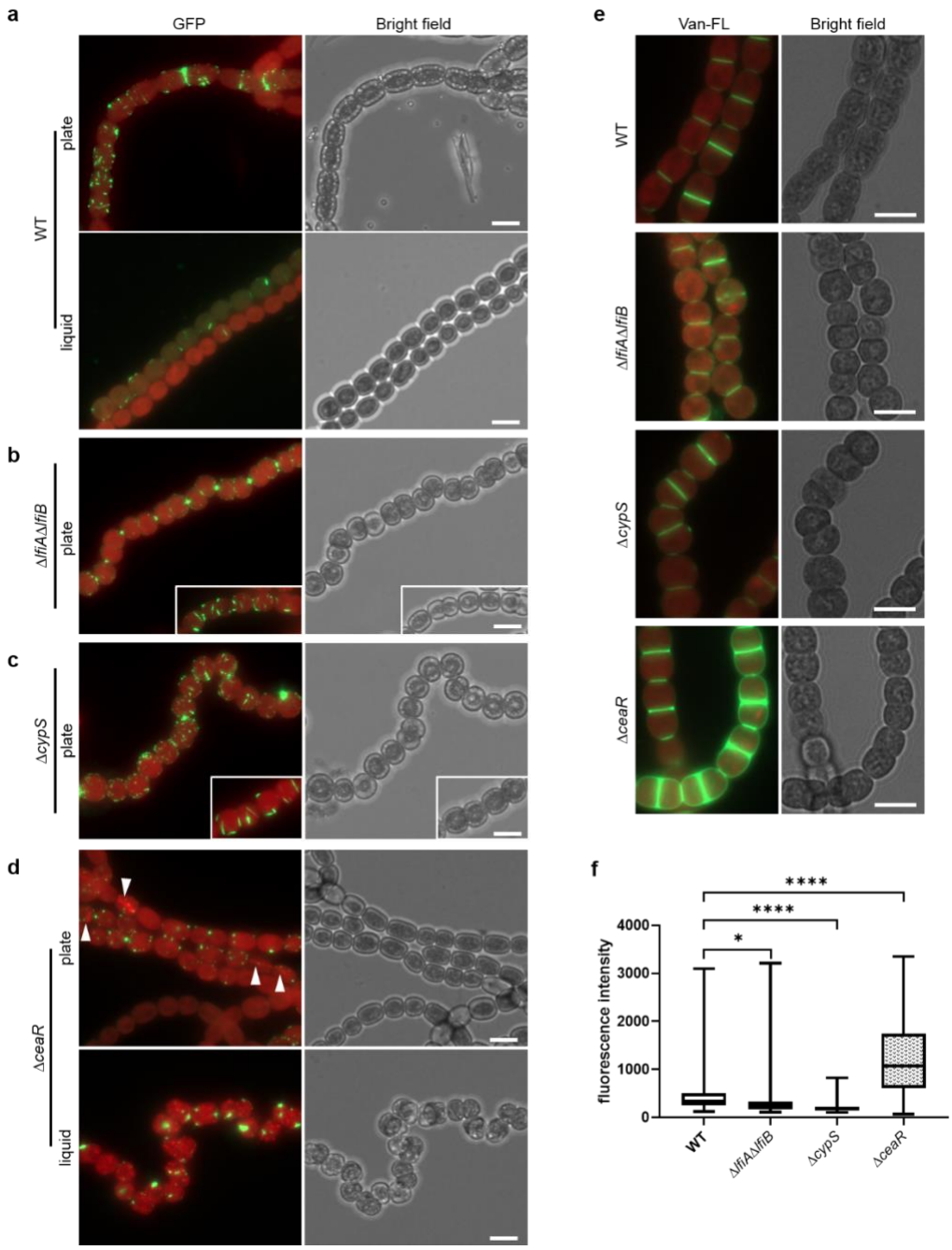

Fig. 3: CCRPs affect MreB localization and PG biogenesis

(**a**-**d**) Merged GFP fluorescence and chlorophyll autofluorescence and bright field micrographs of *Anabaena* WT, Δ*lfiA*Δ*lfiB*, Δ*cypS* and Δ*ceaR* mutant strains expressing GFP-MreB from P_{petE}. Cells were either grown on BG11 plates or in BG11 liquid medium prior visualization. White triangles indicate red fluorescent filaments within Δ*ceaR* mutant cells. Exposure time for GFP fluorescence excitation was 70 ms except for 14 ms in the Δ*ceaR* mutant grown in liquid BG11. Consequently, despite being expressed from the non-native P_{petE}, absence of CeaR detrimentally affects GFP-MreB localization and turnover. (**e**) Merged BODIPY™ FL Vancomycin (Van-FL) fluorescence and chlorophyll autofluorescence and bright field micrographs of *Anabaena* WT, Δ*lfiA*Δ*lfiB*, Δ*cypS* and Δ*ceaR* mutants stained with 1 µg ml^{-1} Van-FL. As a result of the low Van-FL staining and for better visibility, Van-FL fluorescence intensity in Δ*lfiA*Δ*lfiB* and Δ*cypS* was artificially increased about twofold after image acquisition. Unlike in the WT and the other two mutants, Δ*ceaR* mutant cells show longitudinal Van-FL staining, indicating an altered PG biogenesis activity or localization of enzymes involved in PG biogenesis. (**f**) Analysis of the arithmetic mean fluorescence intensities of cells from Fig. 3e. For all measurements, Van-FL fluorescence intensity from cell septa was recorded using 130 ms exposure time from an area of 3.52 $µm^2$. 200 stainings were recorded for each strain. Scale bars: 5 µm.

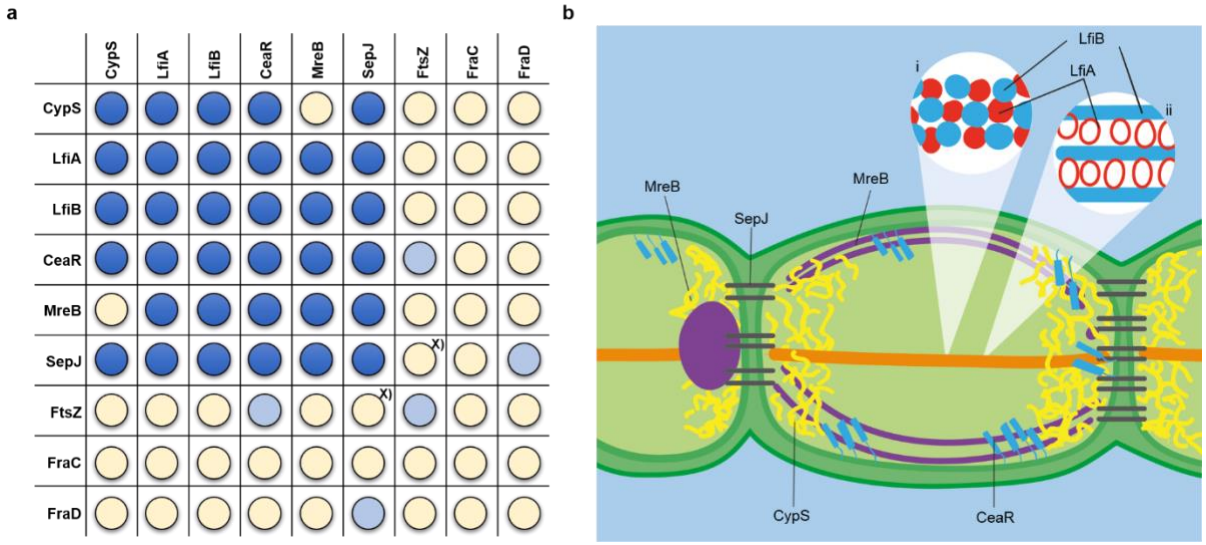

Fig. 4: *Anabaena* CCRPs form a cytoskeletal network that links the septal junction protein SepJ and the MreB cytoskeleton

(**a**) Graphical visualization of beta-galactosidase assay results of *E. coli* BTH101 (Δ*cya*) cells co-expressing indicated translational fusion constructs of *Anabaena* proteins with the T18 and T25 subunit, investigating all possible pair-wise combinations. Corresponding data are shown in Supplementary Fig. 19. Blue spots indicate strong verified interactions (>500 Miller units mg^{-1}) while light blue dots mark moderate interactions (< 500 Miller units mg^{-1}) and no interactions are depicted with yellow-colored dots. Dots marked with "X" were previously reported by Ramos-León *et al.* (2015)[30]. (**b**) A model for an interconnected cytoskeletal network in *Anabaena*. Septal junctions, comprised of, among others, SepJ (grey), are directly connected to the CypS polar scaffold (yellow) that provides anchoring sites for the LfiA/B filament (orange). (i) Similar to α-tubulin and β-tubulin, the LfiA/B heteropolymer could be composed of alternating LfiA (red) and LfiB (blue) monomers. (ii) However, based on *in vivo* localizations, *in vitro* polymerization, domain predictions and structural similarities to eukaryotic plectin, it is more likely that LfiA acts as a cytolinker protein for LfiB, enabling proper polymerization. The LfiA/B filament spans through the cells, anchoring to CypS but never passes through the septal junctions. The identified *Anabaena* filament stabilizing effect of LfiA/B could then be relayed to the neighboring cells via interactions with CypS, CeaR (light blue), SepJ and MreB (purple). MreB localization is adapted from Hu *et al.*[14] in which MreB plugs accumulate at the septa (indicated in the dividing cell on the left) but also forms cell-traversing filaments (right cell). MreB activity and localization is dependent on CeaR. Furthermore, according to FRAP results, it is conceivable that CeaR regulates *Anabaena* filament viability through interaction with SepJ.

References:

1. Young, K. D. The selective value of bacterial shape. *Microbiol. Mol. Biol. Rev.* **70,** 660–703 (2006).

2. Wagstaff, J. & Löwe, J. Prokaryotic cytoskeletons: protein filaments organizing small cells. *Nat. Rev. Microbiol.* (2018). doi:10.1038/nrmicro.2017.153

3. Jones, L. J. F., Carballido-López, R. & Errington, J. Control of cell shape in bacteria: Helical, actin-like filaments in Bacillus subtilis. *Cell* **104,** 913–922 (2001).

4. Bi, E. & Lutkenhaus, J. FtsZ ring structure associated with division in Escherichia coli. *Nature* **354,** 161–164 (1991).

5. Flores, E. *et al.* Septum-localized protein required for filament integrity and diazotrophy in the heterocyst-forming cyanobacterium Anabaena sp. strain PCC 7120. *J. Bacteriol.* **189,** 3884–3890 (2007).

6. Shapiro, J. A. THINKING ABOUT BACTERIAL POPULATIONS AS MULTICELLULAR ORGANISMS. *Annu. Rev. Microbiol.* **52,** 81–104 (1998).

7. Claessen, D., Rozen, D. E., Kuipers, O. P., Søgaard-Andersen, L. & Van Wezel, G. P. Bacterial solutions to multicellularity: A tale of biofilms, filaments and fruiting bodies. *Nat. Rev. Microbiol.* **12,** 115–124 (2014).

8. Reichenbach, H. The ecology of the myxobacteria. *Environ. Microbiol.* **1,** 15–21 (1999).

9. Flärdh, K., Richards, D. M., Hempel, A. M., Howard, M. & Buttner, M. J. Regulation of apical growth and hyphal branching in Streptomyces. *Curr. Opin. Microbiol.* **15,** 737–743 (2012).

10. Flores, E. & Herrero, A. Compartmentalized function through cell differentiation in filamentous cyanobacteria. *Nat. Rev. Microbiol.* **8,** 39–50 (2010).

11. Rossetti, V. & Bagheri, H. C. Advantages of the division of labour for the long-term population dynamics of cyanobacteria at different latitudes. *Proceedings. Biol. Sci.* **279,** 3457–3466 (2012).

12. Herrero, A., Stavans, J. & Flores, E. The multicellular nature of filamentous heterocyst-forming cyanobacteria. *FEMS Microbiol. Rev.* **40,** 831–854 (2016).

13. Zhang, C.-C. C., Hugenin, S., Friry, A., Huguenin, S. & Friry, A. Analysis of genes encoding the cell division protein FtsZ and a glutathione synthetase homologue in the cyanobacterium Anabaena sp. PCC 7120. *Res. Microbiol.* **146,** 445–455 (1995).

14. Hu, B., Yang, G., Zhao, W., Zhang, Y. & Zhao, J. MreB is important for cell shape but not for chromosome segregation of the filamentous cyanobacterium Anabaena sp. PCC 7120. *Mol. Microbiol.* **63,** 1640–1652 (2007).

15. Mullineaux, C. W. *et al.* Mechanism of intercellular molecular exchange in heterocyst-forming cyanobacteria. *EMBO J.* **27,** 1299–1308 (2008).

16. Weiss, G. L., Kieninger, A.-K., Maldener, I., Forchhammer, K. & Pilhofer, M. Structure

and function of a bacterial gap junction analog. *bioRxiv* 462465 (2018). doi:10.1101/462465

17. Lehner, J. *et al.* Prokaryotic multicellularity: A nanopore array for bacterial cell communication. *FASEB J.* **27,** 2293–2300 (2013).

18. Herrmann, H. & Aebi, U. Intermediate Filaments: Molecular Structure, Assembly Mechanism, and Integration Into Functionally Distinct Intracellular Scaffolds. *Annu. Rev. Biochem.* **73,** 749–789 (2004).

19. Ausmees, N., Kuhn, J. R. & Jacobs-Wagner, C. The bacterial cytoskeleton: An intermediate filament-like function in cell shape. *Cell* **115,** 705–713 (2003).

20. Levin, P. A., Kurtser, I. G. & Grossman, A. D. Identification and characterization of a negative regulator of FtsZ ring formation in Bacillus subtilis. *Proc. Natl. Acad. Sci. U. S. A.* **96,** 9642–9647 (1999).

21. Cabeen, M. T. & Jacobs-Wagner, C. Bacterial cell shape. *Nat. Rev. Microbiol.* **3,** 601–610 (2005).

22. Fenton, A. K., Mortaji, L. El, Lau, D. T. C., Rudner, D. Z. & Bernhardt, T. G. CozE is a member of the MreCD complex that directs cell elongation in Streptococcus pneumoniae. *Nat. Microbiol.* **2,** 1–9 (2016).

23. Rojas, E. R. & Huang, K. C. Regulation of microbial growth by turgor pressure. *Curr. Opin. Microbiol.* **42,** 62–70 (2018).

24. Cho, H., Uehara, T. & Bernhardt, T. G. Beta-lactam antibiotics induce a lethal malfunctioning of the bacterial cell wall synthesis machinery. *Cell* **159,** 1310–1311 (2014).

25. Merino-Puerto, V. *et al.* FraC/FraD-dependent intercellular molecular exchange in the filaments of a heterocyst-forming cyanobacterium, Anabaena sp. *Mol. Microbiol.* **82,** 87–98 (2011).

26. Swulius, M. T. & Jensen, G. J. The helical mreb cytoskeleton in Escherichia coli MC1000/pLE7 is an artifact of the N-terminal yellow fluorescent protein tag. *J. Bacteriol.* **194,** 6382–6386 (2012).

27. Leipe, D. D., Wolf, Y. I., Koonin, E. V & Aravind, L. Classification and evolution of P-loop GTPases and related ATPases. *J. Mol. Biol.* **317,** 41–72 (2002).

28. Kerff, F., Terrak, M., Charlier, P., Sauvage, E. & Ayala, J. A. The penicillin-binding proteins: structure and role in peptidoglycan biosynthesis. *FEMS Microbiol. Rev.* **32,** 234–258 (2008).

29. Persat, A. *et al.* The Mechanical World of Bacteria. *Cell* **161,** 988–997 (2015).

30. Ramos-León, F., Mariscal, V., Frías, J. E., Flores, E. & Herrero, A. Divisome-dependent subcellular localization of cell-cell joining protein SepJ in the filamentous cyanobacterium Anabaena. *Mol. Microbiol.* **96,** 566–580 (2015).

Material and methods

Bacterial strains and growth conditions

Anabaena WT was obtained from the Pasteur Culture Collection (PCC) of cyanobacteria (France). Cells were grown photoautotropically in BG11 or without combined nitrogen (BG11-0) at constant light with a light intensity of 30 µmol m^{-2} s^{-1}. When appropriate, 5 µg ml^{-1} spectinomycin (Sp), 5 µg ml^{-1} streptomycin (Sm) or 30 µg ml^{-1} neomycin (Nm) was added to strains carrying respective plasmids or chromosomal insertions. In some cases, basal copper-regulated *petE*-driven expression of gene candidates in *Anabaena* cells was lethal or growth inhibiting, therefore these strains were grown in BG11 (or BG11-0) without copper and protein expression was later induced by the addition of $CuSO_4$ at indicated concentrations to the culture. *E. coli* strains DH5α, DH5αMCR, XL1-blue and HB101 were used for cloning and conjugation by triparental mating. BTH101 was used for BACTH system and BL21 (DE3) was used for expression of His- and GFP-tagged proteins in *E. coli*. All strains were grown in LB medium containing the appropriate antibiotics at standard concentrations. Supplementary Tables 2-5 list all used bacterial strains, plasmids and oligonucleotides.

Prediction of coiled-coil rich proteins

Genome sequence of *Anabaena* (GCA_000009705.1) was analyzed by the COILS algorithm[1] as described by Bagchi et al.[2]. The algorithm was run with a window width of 21 and the cut-off for amino acids in coiled-coil conformation was set to ≥ 80 amino acid residues. The resulting set of protein candidates was further manually examined with online available bioinformatic tools (NCBI Conserved Domain Search, NCBI BLAST, TMHMM Server, PSORTb, I-TASSER). Protein candidates exhibiting BLAST hits involved in cytoskeletal processes or similar domain architectures as known IF proteins like CreS, FilP, vimentin, desmin or keratin were selected, and enzymatic proteins as well as proteins predicted to be involved in other cellular processes were excluded.

Distribution of homologs in cyanobacteria

Cyanobacteria species tree is according to Dagan et al.[3] with the root of the tree as recently inferred by Tria, Landan and Dagan[4]. Homologs to the *Anabaena* proteins were detected by amino acid sequence similarity using stand-alone BLAST[5] ver. 2.2.26. Protein sequences that were found as BLAST hits with a threshold of E-value ≤ $1x10^{-5}$ were further compared to the *Anabaena* protein by global alignment using needle[6]. Hits having ≥30% identical amino acids

in the global alignment were considered as homologs. The phylogenetic tree was visualized with iTOL[7].

Genomic DNA and RNA isolation and cDNA synthesis

Genomic DNA (gDNA) from *Anabaena* was isolated using the GeneJET Plant Genomic DNA Purification Kit (Thermo Fischer Scientific) and the DNeasy Plant Mini Kit (QIAGEN) according to the manufacturer's instructions from 10 ml cyanobacterial cultures.

RNA from *Anabaena* WT (OD_{750} 1.8) was isolated using the Direct-zol™ RNA MiniPrep Kit (Zymo Research) according to the manufacturer's instructions. RNA was isolated in technical triplicates from 10 ml cultures. Isolated RNA was treated with DNA-free™ Kit (2 units rDNAs/reaction; Thermo Fischer Scientific) and 200 ng RNA was reverse transcribed using the qScript™ cDNA Synthesis Kit (Quanta Biosciences). RT-PCR of cDNA samples for *rnpB*, *cypS*, *ceaR*, *lfiA*, *lfiB* and *lfiA*+*lfiB* was done using primer pairs #1/#2, #3/#4, #5/#6, #7/#8, #9/#10, #7/#10, respectively.

Transformation

Transformation of chemically competent *E. coli* was performed by the standard heat shock procedure[8]. *Anabaena* was transformed by triparental mating according to Ungerer and Pakrasi[9]. Briefly, 100 µl of overnight cultures of DH5α carrying the conjugal plasmid pRL443 and DH5αMCR carrying the cargo plasmid and the helper plasmid pRL623, encoding for three methylases, were mixed with 200 µl *Anabaena* culture (for transformation into Anabaena mutant strains, cells were scraped from the plate and resuspended in 200 µl BG11). This mixture was directly applied onto sterilized nitrocellulose membranes placed on top of BG11 plates supplemented with 5% LB medium. Cells were incubated in the dark at 30 °C for 6-8 h with subsequent transfer of the membranes to BG11 plates. After another 24 h, membranes were then transferred to BG11 plates supplemented with the appropriate antibiotics.

Plasmid construction

Ectopic expression of *Anabaena* protein candidates was achieved from a self-replicating plasmid (pRL25C[10]) under the control of the copper-inducible *petE* promoter (P_{petE}) or the native promoter of the respective gene. All constructs were verified by Sanger sequencing (Eurofins Genomics).

Initially, we generated pTHS1 (pRL25C, P_{petE}::*lfiA-gfp)*, which served as template for many other pRL25C-based plasmids employed in this study. For this, P_{petE} and *lfiA* were amplified from *Anabaena* gDNA using primers #11/#12 and #13/#14, respectively. *gfpmut3.1* was amplified from pJET1.2 containing P_{petE}-*gfp*[11] using primers #15/#16. This *gfpmut3.1* (hereafter *gfp*) is deprived of its internal NdeI site and contains a 5' linker sequence of 12 alternating codons encoding for alanine and serine. The PCR fragments were next ligated into PCR-amplified pRL25C (using primers #17/#18) by Gibson assembly.

For pTHS2 (pRL25C, P_{petE}::*lfiB-gfp*) and pTHS3 (pRL25C, P_{petE}::*ceaR-gfp*)*, lfiB* and *ceaR* were amplified from *Anabaena* gDNA using primers #19/#20 or #21/#22, respectively and ligated into PCR-linearized pTHS1 (using primers #23/#24; thereby removing only *lfiA* and leaving P_{petE} and *gfp* in the vector) by Gibson assembly.

For pTHS4 (pRL25C, P_{petE}::*cypS-gfp*), *cypS* was amplified by PCR from *Anabaena* gDNA using primers #36/#38, introducing NdeI and SacI sites, and then ligated into pJET1.2-P_{petE}::*gfp*, thereby generating P_{petE}::*cypS-gfp* which is flanked by a 5' BamHI site and a 3' EcoRI site. The P_{petE}::*cypS-gfp* fragment was excised by BamHI and EcoRI and ligated into BamHI and EcoRI-digested pRL25C.

For pTSH5 (pRL25C, P_{petE}::*trunc-ceaR-gfp*), pTHS3 was amplified using primers #148/#148 and re-ligated using Quick Ligase (NEB). Thereby, the first 153 bp from *ceaR* were removed

For pTHS6 (P_{petE}::*cypS-his*), *cypS-his* was amplified from pTHS8 using primers #25/#26 and ligated into PCR-linearized pRL25C (using primers #24/#27) by Gibson assembly.

For pTHS7 (pRL25C, P_{petE}-*lfiA*-ec*fp,* P_{petE}-*lfiB-gfp*), P_{petE}-*lfiA* was amplified from pTHS1 using primers #28/#29 and ligated into ClaI-digested pRL25C by Gibson assembly together with *myc-link-ecfp* (initially amplified with primers #30/#31, purified and then again amplified with primers #32/#33). This construct was digested by BamHI and ligated by Gibson assembly with PCR-amplified P_{petE}::*lfiB-gfp* from pTHS2 (using primers #34/#35).

pET21a(+) plasmids bearing C-terminal 6His-tag translational fusions of CCRPs were generated by restriction-based cloning techniques. For this, *cypS*, *lfiA*, *lfiB* or *ceaR* were amplified by PCR from *Anabaena* gDNA using primers #36/#37, #39/#40, #41/#42 or #43/#44, respectively, introducing NdeI and XhoI sites. NdeI and XhoI-digested fragments were then ligated into pET21a(+) using Quick Ligase (NEB). This procedure yielded plasmids pTHS8, pTHS9, pTHS10 and pTSH11, respectively.

pET21a(+) bearing C-terminal *gfp* translational fusions were generated based on pTHS12 (pET21a(+), P_{T7}::*cypS-gfp*). For this, *cypS* was amplified by PCR from *Anabaena* gDNA with primers 36#/#38, introducing NdeI and SacI sites, and ligated into NdeI and SacI-digested

pJET1.2 bearing P_{petE}-*gfp*. *cypS-gfp* was excised by NdeI and EcoRI and ligated into NdeI and EcoRI-digested pET21a(+), generating pTHS12. For pTHS13 (pET21a(+), P_{T7}::*ceaR-gfp*), *ceaR-gfp* was amplified by PCR from pTHS3 using primers #47/#48 and ligated into PCR-linearized pTHS12 (primers #49/#50) by Gibson assembly.

GFP-fragment reassembly plasmids were generated by Gibson assembly. For this aim, *lfiA* was amplified by PCR from *Anabaena* gDNA with primer 51/52 or 53/54 and ligated into XhoI and BamHI or NheI digested pET11a-link-NGFP, generating pTHS15 or pTHS16. *lfiB* was amplified by PCR from *Anabaena* gDNA with primers 55/56 and ligated into NcoI and AatII digested pMRBAD-link-CGFP, generating pTHS17.

Clonings for bacterial two-hybrid plasmids were done using Gibson assembly of PCR-linearized pKNT25, pKT25, pUT18 or pUT18C plasmids, using primers #57/#58 for pKNT25 and pUT18, primers #59/#60 for pKT25 and primers 61/62 for pUT18C. For each gene, three primer combinations were used for amplification from *Anabaena* gDNA. The first primer pair was always used for cloning of the respective gene into pKNT25 and pUT18 while the second and third primer pairs were used for cloning into pKT25 or pUT18C, respectively: *cypS* (primers #63/#64, #65/#66 or #67/#68), *lfiA* (primers #69/#70, #71/#72 or #73/#74), *lfiB* (primers #75/#76, #77/#78 or #79/#80), *ceaR* (primers #81/#82, #83/#84 or #85/#86), *sepJ* (primers #87/#88, #89/#90 or #91/#92), *ftsZ* (primers #93/#94, #95/#96 or #97/#98), *mreB* (primers #99/#100, #101/#102 or #103/#104), *fraC* (primers #105/#106, #107/#108 or #109/#110) and *fraD* (primers #111/#112, #113/#114 or #115/#116). This yielded plasmids pTHS17-pTHS52, respectively.

Like for P_{petE}-driven expression, native expression of *Anabaena* CCRPs was mediated from the pRL25C plasmid. For pTHS56 (pRL25C, P_{cypS}::*cypS-gfp*), P_{cypS} was amplified from *Anabaena* gDNA using primers #150/#151 and ligated into BamHI and EcoRI-digested pRL25C by Gibson assembly together with *cypS-gfp*, which was amplified from pTHS4 using primers #152/#153.

For pTHS57 (pRL25C, P_{ceaR}::*ceaR-gfp*), P_{ceaR} was amplified from *Anabaena* gDNA using primers #154/#155 and ligated into BamHI and EcoRI-digested pRL25C by Gibson assembly together with *ceaR-gfp*, which was amplified from pTHS3 using primers #156/#153.

For pTHS58 (pRL25C, P_{lfiA}::*lfiA-gfp*), P_{lfiA} was amplified from *Anabaena* gDNA using primers #157/#158 and ligated into BamHI and EcoRI-digested pRL25C by Gibson assembly together with *lfiA-gfp*, which was amplified from pTHS1 using primers #159/#153.

For pTHS59 (pRL25C, P_{lfiB}::*lfiB-gfp*), P_{lfiB} was amplified from *Anabaena* gDNA using primers #160/#161 and ligated into BamHI and EcoRI-digested pRL25C by Gibson assembly together with *lfiB-gfp*, which was amplified from pTHS2 using primers #162/#153.

For pTHS60 (pRL25C, P_{cypS}::*cypS-his*), P_{cypS} was amplified from *Anabaena* gDNA using primers #150/#151 and ligated into BamHI and EcoRI-digested pRL25C by Gibson assembly together with *cypS-his*, which was amplified from pTHS8 using primers #152/#163.

For pTHS61 (pRL25C, P_{ceaR}::*ceaR*), P_{ceaR}::*ceaR* was amplified from *Anabaena* gDNA using primers #154/#164 and ligated into BamHI and EcoRI-digested pRL25C by Gibson assembly.

For pTHS58 (pRL25C, $P_{lfiA/B}$::*lfiA-lfiB*), $P_{lfiA/B}$::*lfiA-lfiB* was amplified from *Anabaena* gDNA using primers #157/#165 and ligated into BamHI and EcoRI-digested pRL25C by Gibson assembly.

Anabaena mutant strain construction

All *Anabaena* mutant strains were generated using the pRL278-based double homologous recombination system employing the conditionally lethal *sacB* gene[12]. For this, 1500 bp upstream and downstream of the gene to be replaced were generated by PCR from *Anabaena* gDNA. Upstream and downstream regions of *cypS* and *ceaR*, were amplified using primers #121/#122 and #123/#124 or #125/#126 and #127/#128, respectively. Upstream region of *lfiA* was amplified using primers #129/#130 and downstream region of *lfiB* was amplified using primers #131/#132. The respective upstream and downstream homology regions flanking the CS.3 cassette (amplified with primer #119/#120 from pCSEL24) were then inserted into PCR-amplified pRL278 (using primer #117/#118) by Gibson assembly, yielding pTHS55, pTHS56 and pTHS57, respectively. Anabaena transformed with those plasmids was subjected to several rounds of re-streaking on new plates (about 5-8 rounds for each strain). To test for fully segregated clones, colony PCRs were performed after each re-streaking round. For this, *Anabaena* cells were resuspended in 10 µl sterile H_2O of which 1 µl was used for standard PCR with internal gene primers #3/#4, #5/#6 and #7/#10 for Δ*cypS*, Δ*ceaR* and Δ*lfiA*Δ*lfiB,* respectively. Correct placement of the CS.3 cassette was then further confirmed using primers CS.3 cassette primers with primers binding outside of the 5' and 3' flanks used for homologous recombination (#137/#118 and #117/#138 for Δ*cypS*, #135/#118 and #117/#136 for Δ*ceaR* and #133/#118 and #117/#134 for Δ*lfiA*Δ*lfiB*).

Growth curve analysis

For analysis of mutant viability, growth curves of *Anabaena* WT and Δ*ceaR* mutant strain were performed. For this, cells were grown in BG11 liquid medium, washed three times by centrifugation (6500 x *g*, RT, 3 min) in BG11 or BG11-0, adjusted to an OD_{750} of 0.1 and then grown in triplicates at standard growth conditions in 15 ml culture volumes. OD_{750} values were recorded every 24 h for 24 d.

Fluorescence microscopy

Bacterial strains grown in liquid culture were either directly applied to a microscope slide or previously immobilized on a 2% low-melting agarose in PBS (10 mM Na_2HPO_4, 140 mM NaCl, 2.7 mM KCl, 1.8 mM KH_2PO_4, pH 7.4) agarose pad (agarose pad) and air dried before microscopic analysis. Epifluorescence was done using an Axio Imager.M2 light microscope (Carl Zeiss) equipped with Plan-Apochromat 63x/1.40 Oil M27 objective and the AxioCam MR R3 imaging device (Carl Zeiss). GFP, Alexa Fluor 488 and BODIPY™ FL Vancomycin (Van-FL) fluorescence was visualized using filter set 38 (Carl Zeiss; excitation: 470/40 nm band pass (BP) filter; emission: 525/50 nm BP). Chlorophyll auto-fluorescence was recorded using filter set 15 (Carl Zeiss; excitation: 546/12 nm BP; emission: 590 nm long pass). When applicable, cells were previously incubated in the dark at RT for about 5 min with 10 µg ml^{-1} DAPI (final concentration) to stain intracellular DNA. For visualization of DAPI fluorescence filter set 49 (Carl Zeiss; excitation: G 365 nm; emission: 455/50 nm) was employed. For confocal laser scanning microscopy, the LSM 880 Axio Imager 2 equipped with a C-Apochromat 63x/1.2 W Korr M27 objective and an Airyscan detector (Carl Zeiss) was used and visualization of GFP, eCFP and chlorophyll auto-fluorescence was done using Zen black smart setup settings. Also, to investigate putative alterations of the polysaccharide sheath of *Anabaena* mutants, cells were grown on BG11-0 agar plates, re-suspended in BG11-0 liquid medium and stained with 0.05% alcian blue (final concentration). Polysaccharide staining of *Anabaena* cells immobilized on an agarose pad was then observed with an Axiocam ERc 5s color camera (Carl Zeiss). *E. coli* BL21 (DE3) cells expressing C-terminally GFP-tagged protein candidates were were grown over night in LB and then diluted 1:40 in the same medium the following day. Cells were grown for 2 h at 37 °C, briefly acclimated to 20 °C for 10 min and induced with 0.05 mM IPTG at 20 °C. Protein localization of GFP-tagged proteins was then observed after indicated time points of cells immobilized on an agarose pad.

Transmission electron microscopy and sacculi preparation

For ultra-structure analysis, *Anabaena* filaments were fixed with 2.5% glutaraldehyde, immobilized in 2% agaorse, treated with 2% potassium permanganate and dehydrated through a graded ethanol series. The fixed cells were infiltrated by ethanol:EPON (2:1 to 1:2 ratio) and embedded in pure EPON. Ultrathin sections were prepared with a Leica UC6iUltramicrotome, transferred to formvar coated copper grids and post-stained with uranyl acetate and lead citrate[13]. Micrographs were recorded at a Philips Tecnai10 electron microscope at 80 kV.

Peptidoglycan sacculi were isolated from filaments grown on BG11 agar plates by the method of Kühner et al.[14] with the following modifications: Cells were sonicated (Branson Sonifier 250; duty cycle 50%, output control 1, 2 min) prior to boiling in 0.1 M Tris-HCl pH 6.8 with 3% SDS. After incubation in a sonifier waterbath, the samples were incubated with α-Chymotrypsin (600 µg ml^{-1}) at 37 °C over night in 50 mM Na_3PO_4 buffer pH 6.8. After inactivation of the enzyme, the sample was sonified again and loaded on a formvar/carbon film coated copper grid (Science Services GmbH, Munich) and stained with 1 % (w/v) uranyl acetate as described previously[15]. Images were taken with a Philips Tecnai10 electron microscope at 80 kV.

Calcein labeling and fluorescence recovery after photobleaching (FRAP) experiments

Anabaena WT and mutant strains were either grown on BG11 plates and resuspended in BG11 or directly taken from liquid cultures, washed several times in BG11, resuspended in 0.5 ml BG11 and incubated with 10 µl calcein-AM (1 mg ml^{-1} in DMSO). The cells were incubated in the dark at 30 °C for 1 hour and then subjected to four washing steps with 1 ml BG11. Subsequently, cells were resuspended in a small volume of BG11, spotted on BG11 agar plates (1 % w/v) and air dried. Samples were visualized by using an inverted confocal laser scanning microscope (Leica TCS SP5) with a x63 oil immersion objective (HCX PL APO 63x 1.40-0.60 OIL CS). Fluorescence was excited at 488 nm and emission monitored by collecting across a window of 500 to 530 nm with a maximally opened pinhole (600 µm). FRAP experiments were carried out by an automated routine as previously described (Mullineaux *et al.* EMBO). After recording an initial image, selected cells were bleached by increasing the laser intensity by a factor of 5 for two subsequent scans and the fluorescence recovery followed in 0.5 s intervals for 30 s. using the Leica LAS X software. Exchange coefficients (*E*) were then calculated according to Mullineaux *et al*. and Nieves-Morión et al.[16,17].

BODIPY™ FL Vancomycin (Van-FL) staining

Van-FL staining of BG11-grown filaments of the Anabaena WT and mutant strains was essentially performed as previously described by Lehner et al.[18] and Rudolf et al.[19]. Briefly, cells were resuspended in BG11 medium, washed once in BG11 by centrifugation (6500 x *g*, 4 min, RT) and incubated with 1 µg ml^{-1} Van-FL (dissolved in methanol). Cells were incubated in the dark for 1 hour at 30 °C, washed three times with BG11 and immobilized on an agarose pad. Fluorescence signals were then visualized using epifluorescence microscopy. Arithmetic mean fluorescence intensities were then recorded from the septa between two cells with a measured area of 3.52 μm^2 using the histogram option of the Zen blue 2.3 software (Car Zeiss). Excitation time was always 130 ms.

Determination and calculation of cell morphological features

Cell length, volume and roundness were determined using the imaging software ImageJ. Cell volume was calculated based on the assumption of an elliptic cell shape of *Anabaena* cells using the Major Axis and Minor Axis values given by ImageJ and the formula for the volume of an ellipse ($V = \frac{4}{3}\pi abc$):

- $V = \frac{4}{3}\pi\left(\left(\frac{Major\ Axis}{2}\right)^2 \frac{Minor\ Axis}{2}\right)$

Bacterial two-hybrid and beta galactosidase assays

Chemically competent *E. coli* BTH101 (Δ*cya*) cells were co-transformed with 5 ng of plasmids carrying the respective T18 and T25 translational fusion constructs, plated onto LB plates supplemented with 200 µg ml^{-1} X-gal, 0.5 mM IPTG, Amp, Km and grown at 30°C for 24-36 h. Interactions were quantified by beta-galactosidase assays from three independent colonies. For this aim, cultures were either grown over night at 30 °C or for two days at 20 °C in LB Amp, Km, 0.5 mM IPTG and beta-galactosidase activity was recorded as described in the manufacturer's instructions (Euromedex; BACTH System Kit Bacterial Adenylate Cyclase Two-Hybrid System Kit) in a 96 well plate according to Karimova, Davi and Ladant[20].

GFP-fragment reassembly assay

Chemically competent *E. coli* BL21 (DE3) were co-transformed with indicated plasmid combinations, plated on LB Amp, Km and grown over night at 37 °C. Liquid overnight cultures of single colonies of the respective plasmid-bearing *E. coli* strains were then diluted 1:40 in the

same medium the following day. Cells were grown for 2 h at 37 °C, briefly acclimated to 20 °C for 10 min and protein expression was induced with 0.05 mM IPTG and 0.2% L-arabinose. Pictures of induced cultures grown at 20 °C were taken after 48 h of cells immobilized on an agarose pad.

Co-immunoprecipitation

About 20-30 ml of the respective *Anabaena* culture was pelleted by centrifugation (4800 x *g*, 10 min, RT), cells were washed twice by centrifugation (4800 x *g*, 10 min, RT) with 40 ml PBS and then resuspended in 1 ml lysis buffer (PBS-N: PBS supplemented with 1% NP-40) supplemented with protease inhibitor cocktail (PIC; cOmplete™, EDTA-free Protease Inhibitor Cocktail, Sigma-Aldrich). Cells were lysed using the VK05 lysis kit (Bertin) in a Precellys® 24 homogenizer (3 strokes for 30 seconds at 6500 rpm) and cell debris was pelleted by centrifugation (30 min, 21,100 x *g*, 4 °C). 50 µl µMACS anti-GFP MicroBeads (Miltenyi Biotec) was added to the resulting cell-free supernatant and incubated for 1 h at 4 °C with mild rotation. Afterwards, the sample was loaded onto µColumns (Miltenyl Biotec), washed two times with 1 ml lysis buffer and eluted in 50 µl elution Buffer (50 mM Tris HCl pH 6.8, 50 mM DTT, 1% SDS, 1 mM EDTA, 0.005% bromphenol blue, 10% glycerol; Miltenyl Biotec). Until further use, samples were stored at -80 °C.

Mass spectrometry analysis

Coomassie stained gel bands were excised and protein disulfide bonds were reduced with 10 mM dithiotreitol at 56 °C for 45 min and alkylated with 55 mM iodoacetamide at RT for 30 min in the dark. The gel bands were washed 50 mM ammonium bicarbonate and subsequently dehydrated with acetonitrile. 10 µl trypsin (5 ng μl^{-1} in 25 mM ammonium bicarbonate) were added and the gel bands were rehydrated for 5 min at 37 °C. Samples were digested over night at 37 °C.
Prior to peptide extraction samples were acidified with 10% formic acid. After transferring the supernatant into a new Eppendorf tube, 5% formic acid was added to the gel bands and incubated for 10 min. Subsequently the samples were sonicated for 1 min in ice-cooled water and the supernatant was combined with the one from the step before. Two additional extraction steps with 60% acetonitrile/1% formic acid and 100% acetonitrile were performed in the same manner. The combined supernatants were dried in the SpeedVac and the samples were reconstituted in 30 µL 3% acetonitrile/0.1% trifluoroacetic acid.

LC-MS/MS analysis was performed using a Dionex U3000 nanoUHPLC coupled to a Q Exactive Plus mass spectrometer (both from Thermo Scientific). The LC-MS/MS parameters were as follows: Six microliter were injected and loaded on a trap column (Acclaim Pepmap 100 C18, 10 mm × 300 µm, 3 µm, 100 Å, Dionex) and washed for 3 min with 2% ACN/0.05% TFA at a flow-rate of 30 µL min^{-1}. separation was performed using an Acclaim PepMap 100 C18 analytical column (50 cm × 75 µm, 2 µm, 100 Å, Dionex) with a flow-rate of 300 nL/min and following eluents: A (0.05% FA) and B (80% ACN/0.04% FA); linear gradient 5-40% B in 60 min, 50-90% B in 5 min, 90% B for 10 min, 90-5% B in 1 min and equilibrating at 5% B for 11 min. Ionization was performed with 1.5 kV spray voltage applied on a non-coated PicoTip emitter (10 µm tip size, New Objective, Woburn, MA) with the source temperature set to 250°C. MS data were acquired from 5 to 85 min with MS full scans between 300 and 1,800 m/z at a resolution of 70,000 at m/z 200. The 10 most intense precursors with charge states ≥2+ were subjected to fragmentation with HCD with NCE of 27%; isolation width of 3 m/z; resolution, 17,500 at m/z 200. Dynamic exclusion for 30 s was applied with a precursor mass tolerance of 10 ppm. Lock mass correction was performed based on the polysiloxane contaminant signal of 445.120025 m/z. Additional wash runs were performed between samples from gel bands to reduce carry over while cytochrome C was used to monitor mass accuracy and LC quality control.

The acquired MS/MS data were searched with the SequestHT algorithm against the entire reviewed Uniprot protein database of *Nostoc* sp. PCC 7120 including plasmids (6922 sequences in total). Static modifications applied were carbamidomethylation on cysteine residues, while oxidation on methionine residues was set as dynamic modification. Spectra were searched with full enzyme specificity. A MS mass tolerance of 10 ppm and a MS/MS tolerance of 0.02 Da was used. Proteins were identified with at least three unique peptides with a FDR confidence ≤ 0.01 (high).

Immunofluorescence

Immunolocalization of CypS-His and FtsZ in *Anabaena* was essentially performed as described by Ramos-León et al.[21]. For visualization of FtsZ, *Anabaena* WT and mutant strains were streaked from growth plates (BG11 and BG11-0 plates), resuspended in a small volume of distilled water and air-dried on Polysine® adhesion slides (Menzel) at RT followed by fixation and permeabilization with 70% ethanol for 30 min at -20 °C. Cells were allowed to air dry for 30 min at RT and then washed two times with PBST (PBS supplemented with 0.1% (v/v) Tween-20) for 2 min. Unspecific binding sites were blocked for 30 min at RT with blocking buffer (1x Roti®-ImmunoBlock in PBST; Carl Roth) and afterwards rabbit anti-FtsZ (Agrisera; 1:150 diluted) antibody in blocking buffer was added to the cells and incubated for 1.5 h at RT

in a self-made humidity chamber followed by five washing steps with PBST. 7.5 µg ml^{-1} Alexa Fluor488 conjugated goat anti-rabbit IgG (H+L) secondary antibody (Thermo Fischer Scientific) in blocking buffer was added to the cells and incubated for 1 h at RT in the dark in a self-made humidity chamber. Subsequently, cells were washed five times with PBST, air dried and mounted with ProLong™ Diamond Antifade Mountant (Thermo Fischer Scientific) overnight at 4 °C. Immunolocalization of FtsZ was then analyzed by epifluorescence microscopy. Similarly, *in vivo* localization of CypS-His expressed in *Anabaena* was evaluated by immunolocalization of BG11-0 grown liquid cultures, induced with 0.25 µM $CuSO_4$ for two days, and compared to *Anabaena* WT cells using mouse anti-His primary antibody (1:500 diluted; Thermo Fischer Scientific).

Spot assays

Spot assays were essentially performed as described by Dörrich et al.[22]. *Anabaena* WT and mutant strains were grown on BG11 growth plates, resuspended in BG11 liquid medium and adjusted to an OD_{750} of 0.4. Cells were then spotted in triplicates of 5 µl onto the respective growth plates containing either no additives (BG11 or BG11-0), 50 µg ml^{-1} Proteinase K or 100 µg ml^{-1} lysozyme in serial 1/10 dilutions and incubated under standard growth conditions until no further colonies arose in the highest dilution.

Protein purification and *in vitro* filamentation assays

For protein purification, *E. coli* BL21 (DE3) cells carrying His6-tagged protein candidates were grown in overnight cultures at 37 °C and 250 rpm. The next day, overnight cultures were diluted 1:40 in the same medium and grown at 37 °C until they reached an OD_{600} of 0.5-0.6. Protein expression was induced with 0.5 mM IPTG for 3-4 h at 37 °C and 250 rpm. Afterwards, cell suspensions of 50 ml aliquots were harvested by centrifugation, washed once in PBS and stored at -80 °C until further use. For *in vitro* filamentation assays, cell pellets were resuspended in urea lysis buffer (ULB: 50 mM NaH_2PO_4, 300 mM NaCl, 25 mM imidazole, 6 M urea; pH 8.0) and lysed in a Precellys® 24 homogenizer (3x 6500 rpm for 30 s) using the 2 ml microorganism lysis kit (VK01; Bertin) or self-packed Precellys tubes with 0.1 mm glass beads. The resulting cell debris was pelleted by centrifugation at 21,000 x *g* (30 min, 4 °C) and the supernatant was incubated with 1 ml HisPur™ Ni-NTA resin (Thermo Fischer Scientific) for 1 h at 4°C in an overhead rotator. The resin was washed 5 times with 4x resin-bed volumes ULB and eluted in urea elution buffer (UEB: ULB supplemented with 225 mM imidazole). Total protein concentration was measured using the Qubit® 3.0 Fluorometer (Thermo Fischer

Scientific) and generally adjusted to 0.5-1.0 mg ml^{-1} before dialysis. Filament formation of purified proteins was induced by overnight dialysis against polymerization buffer (PLB: 50 mM PIPES, 100 mM KCl, pH 7.0; HLB: 25 mM HEPES, 150 mM NaCl, pH 7.4; or 25 mM HEPES pH 7.5) at 20 °C and 180 rpm with three bath changes using a Slide-A-Lyzer™ MINI Dialysis Device (10K MWCO, 0.5 ml or 2 ml; Thermo Fischer Scientific). Purified proteins were stained with an excess of NHS-Fluorescein (dissolved in DMSO; Thermo Fischer Scientific) and *in vitro* filamentation was analyzed by epifluorescence microscopy.

Material and methods references

1. Lupas, A., Van Dyke, M. & Stock, J. Predicting coiled coils from protein sequences. *Science* **252,** 1162–1164 (1991).

2. Bagchi, S., Tomenius, H., Belova, L. M. & Ausmees, N. Intermediate filament-like proteins in bacteria and a cytoskeletal function in Streptomyces. *Mol. Microbiol.* **70,** 1037–1050 (2008).

3. Dagan, T. *et al.* Genomes of stigonematalean cyanobacteria (subsection V) and the evolution of oxygenic photosynthesis from prokaryotes to plastids. *Genome Biol. Evol.* **5,** 31–44 (2013).

4. Tria, F. D. K., Landan, G. & Dagan, T. Phylogenetic rooting using minimal ancestor deviation. *Nat. Ecol. Evol.* **1,** 0193 (2017).

5. Altschul, S. F., Gish, W., Miller, W., Myers, E. W. & Lipman, D. J. Basic local alignment search tool. *J. Mol. Biol.* **215,** 403–410 (1990).

6. Rice, P., Longden, I. & Bleasby, A. EMBOSS: the European Molecular Biology Open Software Suite. *Trends Genet.* **16,** 276–7 (2000).

7. Letunic, I. & Bork, P. Interactive tree of life (iTOL) v3: an online tool for the display and annotation of phylogenetic and other trees. *Nucleic Acids Res.* **44,** W242–W245 (2016).

8. Sambrook, J. & Green, M. R. *Molecular Cloning: A Laboratory Manual*. (Cold Spring Harbor Laboratory Press, 2012).

9. Ungerer, J. & Pakrasi, H. B. Cpf1 Is A Versatile Tool for CRISPR Genome Editing Across Diverse Species of Cyanobacteria. *Sci. Rep.* **6,** 1–9 (2016).

10. Wolk, C. P. *et al.* Isolation and complementation of mutants of Anabaena sp. strain PCC 7120 unable to grow aerobically on dinitrogen. *J. Bacteriol.* **170,** 1239–1244 (1988).

11. Stucken, K., Ilhan, J., Roettger, M., Dagan, T. & Martin, W. F. Transformation and conjugal transfer of foreign genes into the filamentous multicellular cyanobacteria (subsection V) Fischerella and Chlorogloeopsis. *Curr. Microbiol.* **65,** 552–560 (2012).

12. Cai, Y. & Wolk, C. P. Use of a conditionally lethal gene in Anabaena sp. strain PCC 7120 to select for double recombinats and to entrap insertion sequnces. *J. Bacteriol.* **172,** 3138–3145 (1990).

13. Fiedler, G., Arnold, M., Hannus, S. & Maldener, I. The DevBCA exporter is essential for envelope formation in heterocysts of the cyanobacterium Anabaena sp. strain PCC

7120. *Mol. Microbiol.* **27,** 1193–1202 (1998).

14. Kühner, D., Stahl, M., Demircioglu, D. D. & Bertsche, U. From cells to muropeptide structures in 24 h: Peptidoglycan mapping by UPLC-MS . (2014).

15. Lehner, J. *et al.* The morphogene AmiC2 is pivotal for multicellular development in the cyanobacterium Nostoc punctiforme. *Mol. Microbiol.* **79,** 1655–1669 (2011).

16. Mullineaux, C. W. *et al.* Mechanism of intercellular molecular exchange in heterocyst-forming cyanobacteria. *EMBO J.* **27,** 1299–1308 (2008).

17. Nieves-Morión, M. *et al.* Specific Glucoside Transporters Influence Septal Structure and Function in the Filamentous, Heterocyst-Forming Cyanobacterium Anabaena sp. Strain PCC 7120. *J. Bacteriol.* **199,** e00876-16 (2017).

18. Lehner, J. *et al.* Prokaryotic multicellularity: A nanopore array for bacterial cell communication. *FASEB J.* **27,** 2293–2300 (2013).

19. Rudolf, M. *et al.* The Peptidoglycan-Binding Protein SjcF1 Influences Septal Junction Function and Channel Formation in the Filamentous Cyanobacterium Anabaena *MBio* **6,** e00376-15 (2015).

20. Karimova, G., Davi, M. & Ladant, D. The β-lactam resistance protein Blr, a small membrane polypeptide, is a component of the Escherichia coli cell division machinery. *J. Bacteriol.* **194,** 5576–5588 (2012).

21. Ramos-León, F., Mariscal, V., Frías, J. E., Flores, E. & Herrero, A. Divisome-dependent subcellular localization of cell-cell joining protein SepJ in the filamentous cyanobacterium Anabaena. *Mol. Microbiol.* **96,** 566–580 (2015).

22. Dörrich, A. K., Mitschke, J., Siadat, O. & Wilde, A. Deletion of the Synechocystis sp. PCC 6803 kaiAB1C1 gene cluster causes impaired cell growth under light???dark conditions. *Microbiol. (United Kingdom)* **160,** 2538–2550 (2014).